Reviewer 1

In this manuscript, Pommier et al., report a set of formic acid (HCOOH) enhancement ratios with respect to carbon monoxide (CO) derived from 2008 – 2014 IASI measurements. The authors pay special attention to 7 biomass burning regions comparing their estimates with previous studies. The comparisons show reasonable agreement. In the context of recent studies reporting large underestimations in the HCOOH atmospheric budget (i.e. Stavrakou et al. 2011) the IASI dataset can help to understand a fraction of the underestimation. However for publication in ACP I suggest the paper to undergo major revisions.

The authors would like to thank reviewer 1 for his comments which help to improve our study. We have tried to clarify the points raised by the reviewer and to answer all remarks. Our responses are written in blue in this document.
Sect. 5.1 and 5.2 have been largely rewritten and are not copied in the present replies in full, thus also please read the revised manuscript.

Abstract: With the evidence provided in the text the following sentence is not fully supported "The comparison with other studies highlights a possible underestimation by 60% of emission or a secondary production of HCOOH by Siberian forest fires while the studied fire plumes originating from Southern African savanna could suggests a limited secondary production of HCOOH or a limited sink." The differences in ER between different studies, need to be explained to support such conclusion.
This is a good remark. This statement has been deleted from the abstract, we have however added theses sentences (in bold) in the conclusion:
"The underestimation by 60% over Siberia is consistent with conclusions given in R'Honi et al. (2013). **The calculation of the $ER_{(HCOOH/CO)}$ by biome shows that Siberian plumes are related to the burning of six different vegetation classes. The underestimation reported is thus difficult to confirm without the use of a chemical transport model**."

We have also written in Section 5.2:
"These hypotheses in biased emissions and/or secondary production need, however, to be verified with modeling studies."

Section 4.2: Figure 2 provides a qualitative analysis. HCOOH and CO concentrations apparently track MODIS fire counts. Working out correlations coefficients for CO, HCOOH and fire counts separately will help to address the origin of the air masses and what is the influence of the fire activity on them.
The monthly means does not present a clear correlation as illustrated in Fig. 2 and explained by the sentence in the ACPD manuscript in Section 4.2 (lines 150-152) "It is also worth noting that these variations in the total columns do not depend on the intensity of the fires as shown by Fig. 2 and by the scatterplots with the values characterizing each fire as described below (not shown)."

The impact of the fire activity (FRP) was, however, studied. We did not find correlations between the intensity of each fire and the amount of CO or HCOOH (see Table below for each region) despite that the enhancements in the IASI-derived columns can confidently be attributed to fires. We have decided not to show these results in the manuscript.

region	Criteria: time=[0 5h], r=50km	Criteria: time=[0 5h], r=50km, ws<1.44 m/s
NAF	r (FRP-HCOOH)=0.02 r (FRP-CO)=0.1	r (FRP-HCOOH)=-0.09 r (FRP-CO)=0.13
AMA	r (FRP-HCOOH)=0.03 r (FRP-CO)=0.03	r (FRP-HCOOH)=0.01 r (FRP-CO)=-0.04
AUS	r (FRP-HCOOH)=0.1 r (FRP-CO)=0.08	r (FRP-HCOOH)=0.01 r (FRP-CO)=-0.08
SIB	r (FRP-HCOOH)=0.11 r (FRP-CO)=0.08	r (FRP-HCOOH)=0.2 r (FRP-CO)=0.21
SAF	r (FRP-HCOOH)=0.04 r (FRP-CO)=0.09	r (FRP-HCOOH)=0.05 r (FRP-CO)=0
SEA	r (FRP-CO)=0.13 r (FRP-CO)=0.11	r (FRP-HCOOH)=0.24 r (FRP-CO)=0.18
IND	r (FRP-HCOOH)=0.04 r (FRP-CO)=0.02	r (FRP-HCOOH)=0.08 r (FRP-CO)=0.1

Sections 4.2 and 4.3: The authors try to isolate IASI retrievals influenced by biomass burning using MODIS and ECMWF data. While the definition of the biomass burning regions based in MODIS fire counts is clear, it is not clear to me how co-located IASI data are selected. Quoting the text: "To do so, we co-located the IASI data at 50 km around each MODIS pixel and between 0 and 5h for each detected fire, so that each MODIS pixel is associated with a value of HCOOH and CO total column from IASI".
Further clarification is needed. All these questions are not answered in the description given in the text. For a MODIS pixel is it possible to have more than one IASI retrieval within 50 km? If so, the associated value for that MODIS fire is the average? MODIS has a resolution of 1km by 1km, a given retrieval can be accounted several times due to adjacent MODIS fire pixels. What does it mean 0 and 5 h for each detected fire? 5 hours ahead and 5 hours behind? With MODIS overpass times at 10:30am and 13:30am the night time IASI measurements 9:30pm will always be excluded. What is the influence of modifying the 50 km and 5 hour threshold in the results?

The criteria used correspond to a radius of 50 km around each MODIS hotspot and the time = [0 5h]. Then all the IASI data collocated around each MODIS hotspot were averaged.
To clarify this point we have changed the sentence in the manuscript to:
"To do so, we co-located the IASI data at 50 km around each MODIS pixel and between 0 and 5h from the time registered by MODIS for each detected fire, so that each MODIS pixel is associated with a mean value of HCOOH and CO total columns from IASI".

The idea was to get a sufficient number of hotspots with a high correlation coefficient in order to be confident in the value of the slope $\partial[HCOOH]/\partial[CO]$.
We have chosen to use as temporal criterion +5 hours instead of ±5 hours in order to avoid selecting IASI data before the starting time of a fire. Different criteria on the time difference and the spatial mismatch have been tested in addition to those used in the paper. They are summarized in the Table below but are not shown in the manuscript:

Tab. Correlation coefficients between the HCOOH total columns and the CO total columns measured by IASI for the period between 2008 and 2014 over the seven studied regions, before the use of the wind speed criterion. The results from the criteria, h=[0 5h] and r=50km used in the paper are written in red.

	AMA	AUS	IND	SEA	SAF	NAF	SIB
Criteria used in the paper	0.78 (13342)	0.63 (1525)	0.53 (1641)	0.84 (1865)	0.78 (12227)	0.58 (21139)	0.65 (22353)
h=[0 5h] r=10km	0.72 (1510)	0.49 (114)	0.64 (184)	0.78 (312)	0.69 (1965)	0.42 (2752)	0.39 (2426)
h=[0 10h] r=10km	0.63 (3624)	0.48 (1376)	0.53 (1941)	0.7 (10897)	0.69 (12211)	0.49 (5708)	0.45 (6342)
h=[0 10 h] r=50km	0.73 (32463)	0.61 (12414)	0.47 (20090)	0.74 (87378)	0.72 (124784)	0.6 (58273)	0.66 (46081)
h=[-5h +5h] r=50 km	0.79 (253188)	0.74 (33303)	0.55 (42924)	0.82 (123243)	0.81 (504733)	0.53 (439994)	0.61 (78570)

Concerning the MODIS overpass, it was an error in the text. The correct sentence and overpasses are:
"The Terra and Aqua satellites equatorial overpass times are ~10:30 (am and pm) and ~01:30 (am and pm) local time, respectively."

Surface ECMWF winds definitely increase the confidence of using only biomass burning affected IASI retrievals. However, the sensitivity of the IASI retrievals is highest between 1km and 6km. The authors should address the uncertainties introduced in the calculations due to transport vs. lofting of the air masses and influence of non-pyrogenic air masses in the IASI retrievals. This is particularly relevant for regions other than Equatorial Africa and South Africa were biomass burning signal is superimposed with other sources (Chaliyakunnel et al., 2016).

The impact of the air masses on the IASI CO and HCOOH retrievals represents a specific study which should be done but it is beyond the scope of this paper, even if it is a relevant question. However, to answer this question, we have analyzed the vertical velocity at 1000hPa provided by ECMWF and the wind speed at three levels: 825, 650 and 450 hPa. These fields have the same resolution of the data used in the paper, i.e. 0.125° × .0.125° and a 6h time step. We have checked their impact on our scatterplots as done with the surface wind speed in the manuscript.

The question about the lofting of the air masses can be studied with the vertical velocity. We have plotted the distribution over the seven regions as in figure 3 of the paper and presented hereafter:

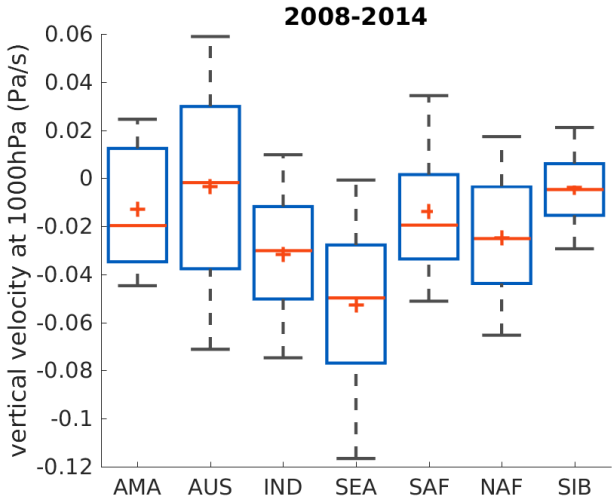

Fig. 1. Box and whisker plots showing mean (red central cross), median (red central line), and 25th and 75th percentile (blue box edges) of vertical velocity at 1000 hPa for each MODIS hotspot over the studied regions (AMA=Amazonia, AUS=Australia, IND = India, SEA = Southern East Asia, NAF= Northern Africa, SAF= Southern Africa, SIB= Siberia).

Since pressure decreases with height, negative values of the vertical velocity indicate rising motion in the atmosphere, and positive values indicate sinking air.
As shown by this figure 1, no clear relationship between the vertical velocity and the correlation found over the regions studied in our work is found. India showing a low correlation coefficient as presented in Tab. 1, does not show a particular difference with other regions. For example, SAF having a lower mean velocity and SEA having a higher mean velocity than IND, have a higher correlation coefficient than IND.
We can conclude that the vertical injection ("lofting of the air masses") has a negligible impact on our scatterplots.
It however suggests a higher rising motion of the air masses over IND and SEA as already stated in Sect. 5.2. We have decided to add this sentence (in bold):
"…this may suggests that the plumes studied over the 7-yr period correspond to fresh plumes where the chemistry or the physical sink is small. **This is further supported by the fact that among the seven regions, IND and SEA have larger vertical velocity means close to the surface indicating a larger rising motion of the air masses (not shown)**."

In order to estimate the impact of the long-range transport on our correlation coefficients, a similar methodology has been used with the wind at different pressure levels.
We chose 450, 650 and 825 hPa, corresponding approximately to 5.7, 3.1 and 1.4 km and the results are presented in Fig. 2 hereafter. These levels are within the range of vertical sensitivity of the IASI HCOOH retrieval, i.e. between 1 and 6 km. The regions showing the lowest correlation coefficient (Tab.1 in the manuscript) do not match with a high or low wind speed. It is however shown that a high mean and median wind speed are noticed over IND and SEA.
These distributions do not allow the identification of a clear influence of the long-range transport in our scatterplots.

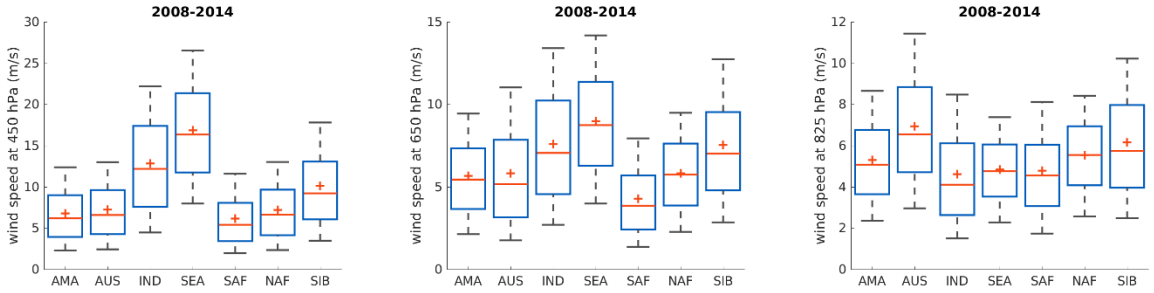

Fig. 2. Box and whisker plots showing mean (red central cross), median (red central line), and 25th and 75th percentile (blue box edges) of wind speed at 450, 650 and 825hPa for each MODIS hotspot over the studied regions (AMA=Amazonia, AUS=Australia, IND = India, SEA = Southern East Asia, NAF= Northern Africa, SAF= Southern Africa, SIB= Siberia).

We have added these sentences in Sect. 4.3:
"It is also noteworthy that the IND and SEA regions are both characterized by higher wind speed at higher altitudes, i.e. for the pressure levels 650 and 450 hPa (not shown). This shows that the wind speed at higher altitudes has a lower influence on our correlations than the surface wind."

Table 1 and 2 can be combined in one single table.
It is a good suggestion. Both tables are now merged as below:

Table 1 Upper row: Correlation coefficients between the HCOOH total columns and the CO total columns measured by IASI for the period between 2008 and 2014 over the seven studied regions. Lower row: As upper row but with only MODIS fire hotspot having a surface wind speed lower than 1.44 m/s. Each IASI data is selected in an area of 50 km around the MODIS fire hotspot and up to 5h after the time recorded for each fire. The number of fires characterized by HCOOH and CO total columns is given in parenthesis.

	AMA	AUS	IND	SEA	SAF	NAF	SIB
r	0.78 (13342)	0.63 (1525)	0.53 (1641)	0.84 (1865)	0.78 (12227)	0.58 (21139)	0.65 (22353)
	0.79 (4580)	0.65 (93)	0.65 (340)	0.86 (528)	0.80 (895)	0.53 (1095)	0.72 (2097)

Sections 5.1 & 5.2: What is the reason for the exception in Siberia where using only columns with a thermal contrast larger than 10K changed the ER from 6.5 mol/mol to 4.4 mol/mol.
More explanations are now given and the new paragraph is (the modifications are highlighted in bold):
"Nevertheless, in order to investigate the possible impact of the overestimation in the lower columns **and the underestimation in the higher columns** on the calculated ratios, a test was performed, by using only HCOOH columns with a thermal contrast larger than 10K. Indeed, the increase in the thermal contrast (i.e. the temperature difference between the surface and the first layer in the retrieved profile) leads to **reducing** the detection limit as shown in Pommier al. (2016**). This enhancement of the detection level helps to minimize the bias in the retrieved total columns as explained in Crevoisier et al. (2014). For the analysis performed here, similar slopes and correlation coefficients were generally calculated**, suggesting a negligible effect of this parameter on the biases. The only exception is an increase in $ER_{(HCOOH/CO)}$ over **Siberia ($6.5\times10^{-3} \pm 0.19\times10^{-3}$ mol/mol when using only IASI**

measurements with TC above 10K against 4.4×10^{-3} mol/mol ± 0.09×10^{-3} in Table 2). It is worth noting that only 48% of the selected scenes remain over Siberia when applying this filter on thermal contrast (60% for SEA, 77% for AMA, 80% for SAF, 83% for AUS and NAF, and 89% for IND). This implies that the statistics on the fire emissions in the higher latitudes of Siberia is dominated by measurements with a low thermal contrast and thus with HCOOH total columns with higher uncertainties. However, the limited changes in slopes and correlation coefficients give us confidence that the results presented in Table 2 are **representative**."

Ground based FTIR, IASI, ACE-FTS, TES, and airborne FTIR are sensitive to different altitudes. The good agreement over Southern Africa can be linked with the distinctive burning season and air masses not containing other origins. That can explain why when ACE-FTS samples air masses that have travelled across the Atlantic Ocean (Risland et al., 2006) the ER are significant. Therefore, to extract quantitative conclusions from the comparison exercise, it is necessary to have information about the origin of the air masses and the type of fuel burned. The authors can address these two issues using back trajectory model, for example Hysplit, and MODIS land surface type. As the manuscript stands now the discussion is mostly speculative.
It is a good remark from the reviewer.

As there are 9628 MODIS hotspots studied in this paper, it is difficult to calculate backward trajectories for each hotspot, especially as different altitude ranges need to be tested since the vertical sensitivity of IASI (CO & HCOOH) is located in the free troposphere.
In order to investigate this, a few tests were done to show the distinct origins of the air masses at different locations, periods of the year and altitudes of the plume. Specifically 5 hotspots have been chosen randomly for each region and 3 different altitudes have been used: 500 m (thus close to the surface), 2000 m and 5000 m (representing the free troposphere). In total, this represents 105 trajectories.
These trajectories show that the air masses initialized at 500 and 2000m are mainly influencing by air masses close to the surface, confirming an origin near the source of our IASI fire-affected columns. It also shows the difficulty to estimate the origin of the air masses without an accurate knowledge of the altitude of the plumes.
These trajectories were plotted through the HYSPLIT online service:

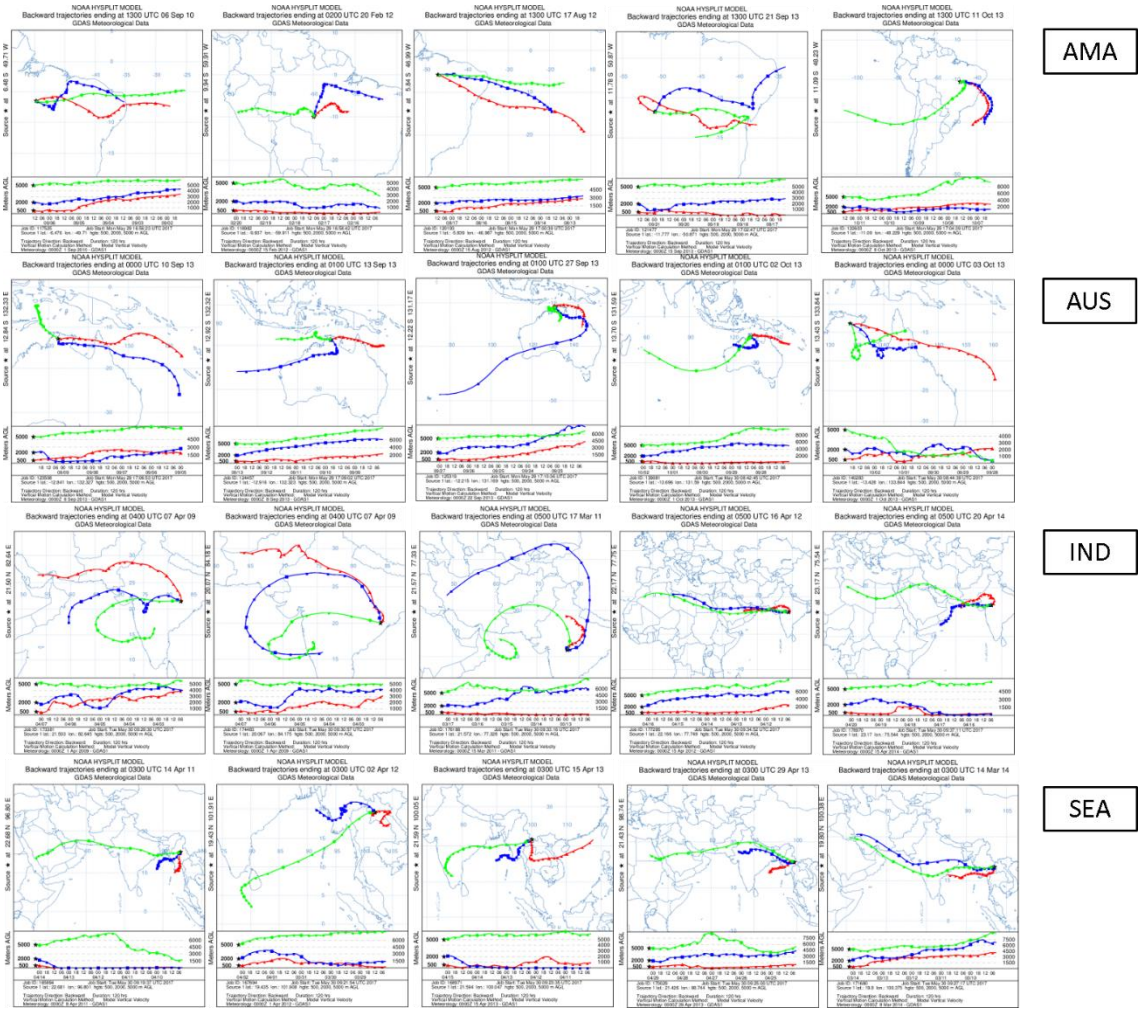

Fig 3. 5-day backward trajectories from HYSPLIT online service calculated at 3 altitudes: 500 m (red), 2000 m (blue) and 5000 m (green), for 5 hotspots chosen randomly over the 7 regions studied in the paper. The parameters characterizing each MODIS hotpots are summarized in the following table. The meteorological fields are from GDAS at 1°×1° horizontal resolution.

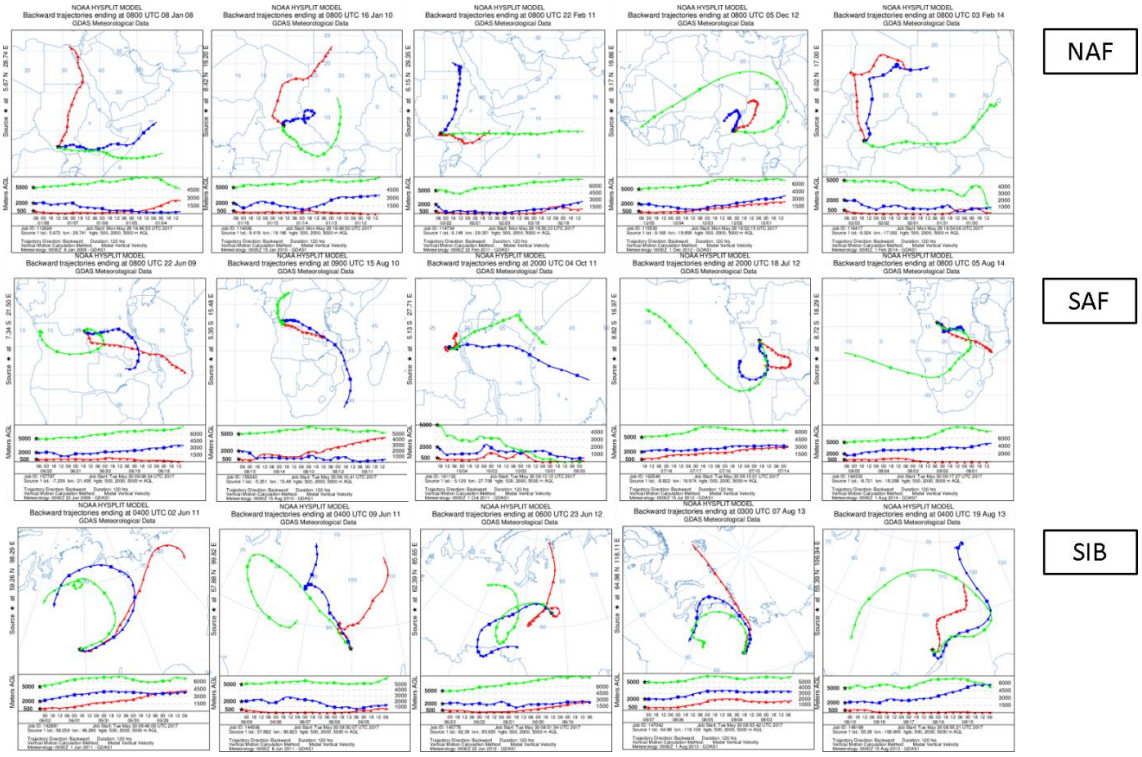

Fig 3. Continue

Tab. Characteristic of each MODIS hotspot used for the trajectories plotted in the previous figure. The dates, the time recorded by the instrument and the coordinates for each hotspot are written.

AMA
20100906 / hour (UTC)=13 / lat=-6.476 - lon=-49.71
20120220 / hour (UTC)=2 / lat=-9.937 - lon=-59.911
20120817 / hour (UTC)=13 / lat=-5.839 - lon=-46.987
20130921 / hour (UTC)=13 / lat=-11.777 - lon=-50.871
20131011 / hour (UTC)=13 / lat=-11.09 - lon=-48.229
AUS
20130910 / hour (UTC)=0 / lat=-12.841 - lon=132.327
20130913 / hour (UTC)=1 / lat=-12.916 - lon=132.323
20130927 / hour (UTC)=1 / lat=-12.215 - lon=131.169
20131002 / hour (UTC)=1 / lat=-13.696 - lon=131.59
20131003 / hour (UTC)=0 / lat=-13.428 - lon=133.844
IND
20090407 / hour (UTC)=4 / lat=21.503 - lon=82.645
20090407 / hour (UTC)=4 / lat=20.067 - lon=84.175
20110317 / hour (UTC)=5 / lat=21.572 - lon=77.328
20120416 / hour (UTC)=5 / lat=22.166 - lon=77.749
20140420 / hour (UTC)=5 / lat=23.17 - lon=75.544
SEA
20110414 / hour (UTC)=3 / lat=22.681 - lon=96.801
20120402 / hour (UTC)=3 / lat=19.435 - lon=101.908
20130315 / hour (UTC)=3 / lat=21.594 - lon=100.047
20130329 / hour (UTC)=3 / lat=21.426 - lon=98.744
20140314 / hour (UTC)=3 / lat=19.8 - lon=100.375

NAF
20080108 / hour (UTC)=8 / lat=5.672 - lon=28.741
20100116 / hour (UTC)=8 / lat=8.419 - lon=19.196
20110222 / hour (UTC)=8 / lat=6.148 - lon=29.351
20121205 / hour (UTC)=8 / lat=9.168 - lon=19.859
20140203 / hour (UTC)=8 / lat=6.024 - lon=17.002
SAF
20090622 / hour (UTC)=8 / lat=-7.339 - lon=21.495
20100815 / hour (UTC)=9 / lat=-5.351 - lon=15.48
20111004 / hour (UTC)=20 / lat=-5.129 - lon=27.708
20120718 / hour (UTC)=20 / lat=-8.822 - lon=16.974
20140805 / hour (UTC)=8 / lat=-8.721 - lon=18.288
SIB
20110602 / hour (UTC)=4 / lat=59.259 - lon=98.286
20110609 / hour (UTC)=4 / lat=57.882 - lon=99.823
20120623 / hour (UTC)=6 / lat=62.39 - lon=85.655
20130807 / hour (UTC)=3 / lat=64.98 - lon=118.109
20130819 / hour (UTC)=4 / lat=55.39 - lon=106.945

To reply to this point, we have added the following sentences (in bold) in the text:
"A few backward trajectories (along 5 days, not shown) have been calculated for our hotspots with the online version of the HYSPLIT atmospheric transport and dispersion modeling system (Rolph, 2017). These trajectories, initialized at different altitudes, confirm a main origin close to the surface of our IASI fire-affected columns. It is however impossible to properly compare the origin of the air masses with previous studies as our studied period (2008-2014) or our studied fires do not necessarily match with plumes described in other publications. It is also difficult to estimate the age of our studied air masses by gathering the plumes during a 7-yr period and without an accurate knowledge of the altitude of the plumes."

And:

"One possible explanation is the multi-origin of the plumes studied by Rinsland et al. (2006), since, based on their backward trajectories, their plumes could be influenced by biomass burning originating from Southern Africa and/or from Southern America. **The travel during the few days across the Atlantic Ocean may explain the change in their $ER_{(HCOOH/CO)}$."**

With the corresponding reference:
Rolph, G.D.: Real-time Environmental Applications and Display sYstem (READY) Website (http://www.ready.noaa.gov). NOAA Air Resources Laboratory, College Park, MD, 2017.

About the type of fuel burned, thanks to the reviewer, we have discovered that such information was available from the MODIS products.
Now, in Section 3. MODIS we have added this paragraph:
"To characterize each MODIS hotspot by the type of fuel burned, the Global Mosaics of the standard MODIS land cover type data product (MCD12Q1) in the IGBP Land Cover Type Classification (Friedl et al., 2010; Channan et al., 2014) with a 0.5° × 0.5° horizontal resolution has also been used (http://glcf.umd.edu/data/lc/). As the annual variability in this product is

limited (not shown) and since the period available (from 2001 to 2012) does not fully match the period of the IASI mission, only the data for 2012 have been used. Whitburn et al. (2017) have also used this MCD12Q1 product to determine their IASI-derived NH_3 enhancement ratios by vegetation types."

With the corresponding references:

Channan, S., Collins, K., and Emanuel, W. R., Global mosaics of the standard MODIS land cover type data. University of Maryland and the Pacific Northwest National Laboratory, College Park, Maryland, USA, 2014.

and

Friedl, M. A., Sulla-Menashe, D., Tan, B., Schneider, A., Ramankutty, N., Sibley, A. and Huang, X., MODIS Collection 5 global land cover: Algorithm refinements and characterization of new datasets, 2001-2012, Collection 5.1 IGBP Land Cover, Remote Sensing of Environment, 114 , 168–182, doi:10.1016/j.rse.2009.08.016, 2010.

and

Whitburn, S., Van Damme, M., Clarisse, L., Hurtmans, D., Clerbaux, C., and Coheur, P.-F.: IASI-derived NH3 enhancement ratios relative to CO for the tropical biomass burning regions, Atmos. Chem. Phys. Discuss., https://doi.org/10.5194/acp-2017-331, in review, 2017.

We have also added this sentence in Section 4.2:

"The classification of the vegetation from the MODIS product has also been used for a detailed analysis of the enhancement ratios for these regions (Fig. 1)."

And Fig. 1 has been modified as below:

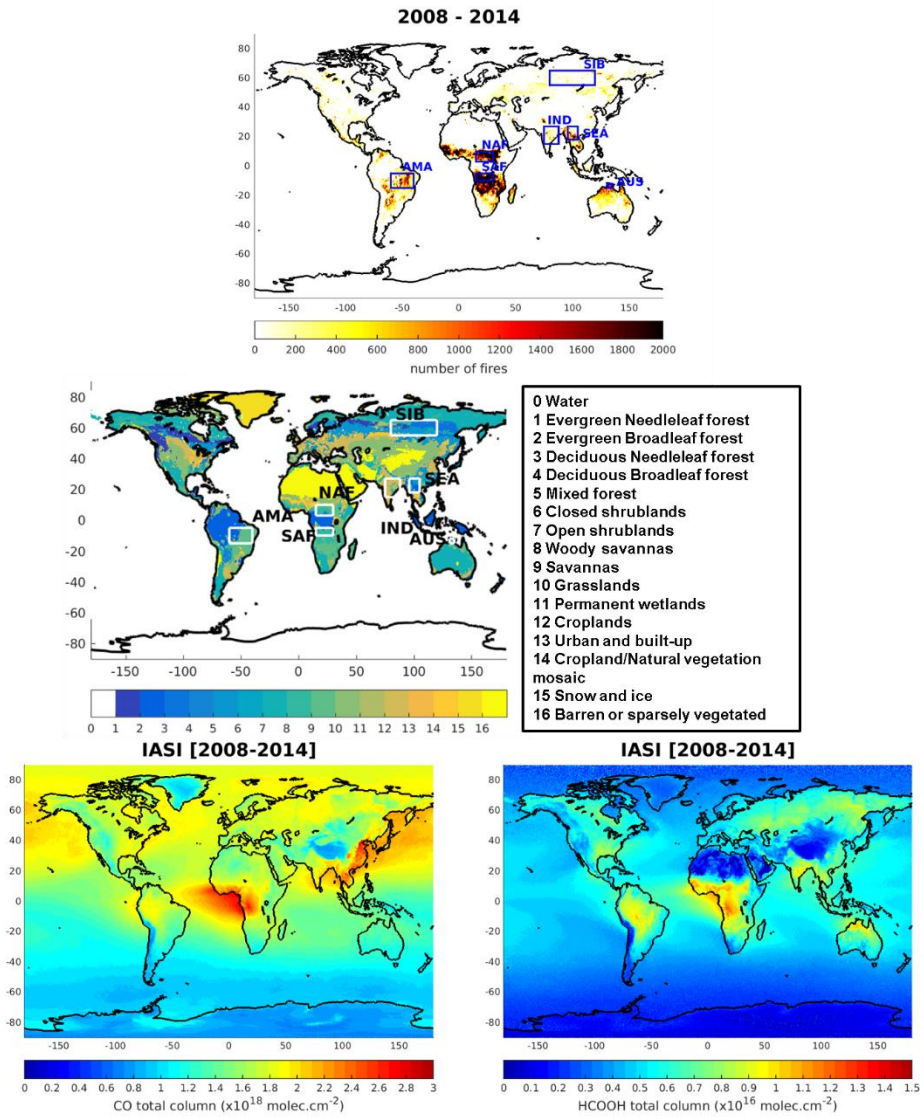

Figure 1: Top: Number of MODIS fire hotspots with a confidence percentage higher or equal to 80%, averaged on a 0.5°×0.5° grid, for the period between 2008 and 2014. The blue boxes are the regions studied in this work. Middle: Classification of the land cover type from MODIS on the same grid and highlighting the studied regions in white. Each number corresponds to the type of vegetation. Only the data between 64°S and 84°N are available. Bottom: The IASI CO total column distribution (left) and the IASI HCOOH total column distribution (right), averaged between 2008 and 2014 and on the same grid.

Section 5.2 was also rewritten and now named "5.2. Analysis based on the type of vegetation" since ER (HCOOH/CO) by type of vegetation were also added in Table 3 as below:

Table 3. Enhancement ratio of HCOOH relative to CO (mol/mol) with its standard deviation and enhancement ratio of HCOOH relative to CO (mol/mol) by biome with its standard deviation calculated in this work. For each enhancement ratio by biome, the correlation coefficient and the number of MODIS hotspots are provided. The enhancement ratios are compared to emission ratios calculated from emission factors given in the literature for the seven studied regions. For the calculation of these emission ratios, the emission factors of CO for the corresponding fuel type given in Akagi et al. (2011) are used. Emission ratios of HCOOH relative to CO (mol/mol) calculated from the emission factors of HCOOH given in Akagi et al. (2011) for the corresponding fuel type are also provided.

Region	**Enhancement Ratio to CO (mol/mol) – this work**	**Enhancement Ratio to CO (mol/mol)[1] by biome[2] – this work**	Emission Ratio to CO (mol/mol) calculated from EF_{HCOOH} given in literature and using EF_{CO} from Akagi et al. (2011)	Instrument used
AMA	**$7.3\times10^{-3} \pm 0.08\times10^{-3}$**	**$6.3\times10^{-3} \pm 0.22\times10^{-3}$ (Evergreen Broadleaf forest, r=0.81, n = 454)** **$3.0\times10^{-3} \pm 0.81\times10^{-3}$ (Open shrubland, r=0.91, n = 5)** **$7.0\times10^{-3} \pm 2.47\times10^{-3}$ (Woody savanna, r=0.63, n = 14)** **$7.6\times10^{-3} \pm 0.09\times10^{-3}$ (Savanna, r=0.79, n = 3909)** **$8.4\times10^{-3} \pm 0.39\times10^{-3}$ (Grassland, r=0.88, n = 143)** **$4.6\times10^{-3} \pm 0.35\times10^{-3}$ (Cropland, r=0.88, n = 54)**	1.8×10^{-3} – Tropical forest (Yokelson et al., 2007 ; 2008)[3] 2.7×10^{-3} – Savanna (Yokelson et al., 2007 ; 2008)[3] 2.0×10^{-3} – Savanna (Akagi et al., 2011) 5.2×10^{-3} – Tropical forest (Akagi et al., 2011)	Airborne FTIR (Yokelson et al., 2007) ; laboratory (Yokelson et al., 2008) catalogue
AUS	**$11.1\times10^{-3} \pm 1.37\times10^{-3}$**	**$5.7\times10^{-3} \pm 2.55\times10^{-3}$ (Woody savanna, r=0.6, n = 11)** **$11.2\times10^{-3} \pm 1.49\times10^{-3}$ (Savanna, r=0.65, n = 80)**	2.0×10^{-3} – Savanna (Akagi et al., 2011)	catalogue
IND	**$6.8\times10^{-3} \pm 0.44\times10^{-3}$**	**$6.6\times10^{-3} \pm 0.77\times10^{-3}$ (Woody savanna, r=0.65, n = 103)** **$6.2\times10^{-3} \pm 0.62\times10^{-3}$ (Cropland, r=0.58, n = 198)** **$8.8\times10^{-3} \pm 1.19\times10^{-3}$ (Cropland/Natural vegetation mosaic, r=0.85, n =23)**	2.0×10^{-3} – Savanna (Akagi et al., 2011) 2.7×10^{-3} – Extratropical forest (Akagi et al., 2011) 6.0×10^{-3} – Cropland (Akagi et al., 2011)	catalogue
SEA	**$5.8\times10^{-3} \pm 0.15\times10^{-3}$**	**$5.6\times10^{-3} \pm 0.20\times10^{-3}$ (Evergreen Broadleaf forest, r=0.83, n = 334)**	2.0×10^{-3} – Savanna (Akagi et al., 2011) 2.7×10^{-3} – Extratropical forest (Akagi et al., 2011) 6.0×10^{-3} – Cropland (Akagi et al., 2011)	catalogue

		$6.3\times10^{-3} \pm 0.66\times10^{-3}$ (Mixed forest, r=0.76, n = 70) **$6.2\times10^{-3} \pm 0.38\times10^{-3}$ (Woody savanna, r=0.86, n = 99)** **$7.1\times10^{-3} \pm 0.99\times10^{-3}$ (Cropland/Natural vegetation mosaic, r=0.84, n =23)**		
NAF	**$4.0\times10^{-3} \pm 0.19\times10^{-3}$**	**$3.4\times10^{-3} \pm 0.63\times10^{-3}$ (Evergreen Broadleaf forest, r=0.52, n = 78)** **$3.3\times10^{-3} \pm 0.28\times10^{-3}$ (Woody savanna, r=0.44, n = 569)** **$4.4\times10^{-3} \pm 0.29\times10^{-3}$ (Savanna, r=0.59, n = 441)** **$22.6\times10^{-3} \pm 11.06\times10^{-3}$ (Cropland/Natural vegetation mosaic, r=0.67, n = 7)**	2.0×10^{-3} – Savanna (Akagi et al., 2011)	catalogue
SAF	**$5.0\times10^{-3} \pm 0.13\times10^{-3}$**	**all hotspots are woody savanna**	3.3×10^{-3} – Tropical forest (Sinha et al., 2004)[4] 4.8×10^{-3} – Savanna (Sinha et al., 2004)[4] 4.1×10^{-3} – Tropical forest (Yokelson et al., 2003) 6.0×10^{-3} – Savanna (Yokelson et al., 2003) 13×10^{-3} – Tropical forest (Rinsland et al., 2006) 19.2×10^{-3} – Savanna (Rinsland et al., 2006) 2.0×10^{-3} – Savanna (Akagi et al., 2011) 5.2×10^{-3} – Tropical forest (Akagi et al., 2011)	Airborne FTIR Airborne FTIR ACE-FTS catalogue
SIB	**$4.4\times10^{-3} \pm 0.09\times10^{-3}$**	**$4.0\times10^{-3} \pm 0.31\times10^{-3}$ (Evergreen Needleaf forest, r=0.63, n = 245)** **$3.6\times10^{-3} \pm 0.16\times10^{-3}$ (Deciduous Needleaf forest, r=0.66, n = 659)** **$3.4\times10^{-3} \pm 0.18\times10^{-3}$ (Mixed forest, r=0.57, n = 759)**	2.7×10^{-3} – Boreal forest (Akagi et al., 2011)	catalogue

	$6.6\times10^{-3} \pm 0.48\times10^{-3}$ (Open shrubland, r=0.76, n = 143) **$6.0\times10^{-3} \pm 0.41\times10^{-3}$ (Woody savanna, r=0.76, n = 155)** **$3.8\times10^{-3} \pm 0.65\times10^{-3}$ (Permanent wetland, r=0.6, n = 63)**

[1] Only the enhancement ratio to CO calculated from a scatterplot with a correlation coefficient higher than 0.4 are reported.
[2] The type of vegetation is defined by the land cover type data product (MCD12Q1).
[3] The EF_{HCOOH} were corrected based on the comment from Yokelson et al. (2013) (EF_{HCOOH} used: 0.281 for Yokelson et al. (2007); 0.2767 for Yokelson et al. (2008)).
[4] The mean of both EF_{HCOOH} values provided in Sinha et al. (2004) were used for our $EmR_{HCOOH/CO}$ calculation

We have added these sentences at the end of the Section 5.2:
"In addition to the $EmR_{(HCOOH/CO)}$ calculated from the EF_{HCOOH} given in the literature, a classification for our $ER_{(HCOOH/CO)}$ has also been done, based on the data from the MCD12Q1 product. As each hotspot is associated with a land cover value defined by the MCD12Q1 product, enhancement ratios by biome have been calculated. The limitations of this dataset are its coarse resolution (0.5° × 0.5°) and the lack of seasonal variation. It gives however a supplementary information on the type of fuel burned identified by MODIS. The corresponding $ER_{(HCOOH/CO)}$ are provided in Table 3. Only the values calculated from a scatterplot with a correlation coefficient higher than 0.4 are reported."

And

"In general, the $ER_{(HCOOH/CO)}$ calculated for a specific biome varies with the regions. This shows that the type of vegetation is not the only factor influencing the $ER_{(HCOOH/CO)}$. The ongoing chemistry within a plume is important and the age of the air masses impact the level of HCOOH and CO in the plumes."

We have also added these sentences in the abstract:
"An additional classification of the enhancement ratios by type of fuel burned is also provided, showing a diverse origin of the plumes sampled by IASI, especially over Amazonia and Siberia. The variability in the enhancement ratios by biome over the different regions show that the levels of HCOOH and CO do not only depend on the fuel types."
And in the conclusion:
"Finally, the estimation of the $ER_{(HCOOH/CO)}$ calculated by the type of vegetation burned, as referenced in the MODIS product, varies with the regions. This shows that other parameters than the type of fuel burned also influence the $ER_{(HCOOH/CO)}$."

Conclusions: As with the abstract "Fires over Australia and over Siberia are probably underestimated in terms of direct emission or secondary production of HCOOH. The analysis over Australia is however delicate as our ER (HCOOH/CO) approximately corresponds to the mean of the values reported in Paton- Walsh et al. (2005) and in Chaliyakunnel et al. (2016); and is also 450% higher than the E m R (HCOOH/CO) derived from Akagi et al. (2011). The underestimation by 60% over Siberia is consistent with conclusions given in R'Honi et al., (2103)." a more detailed analysis is needed to link differences in ER with direct emission and secondary production.

It is correct. See our responses to your first comment (abstract).

Finally, IASI is also capable of measuring HCN a useful biomass burning tracer. It will be useful if the authors discussed the possibility of using it in future analysis.
It is a good remark. This sentence has been modified (in bold) in the conclusion:
"This IASI data set may also be used in the future to study a single plume at different times **to inform on the loss during transport. Further insight into the transport and chemistry may be gained by using IASI's capability to measure several fire species simultaneously, such as HCN or C_2H_2 (e.g. Duflot et al., 2015**)."

The corresponding reference has also been added:
Duflot, V., Wespes, C., Clarisse, L., Hurtmans, D., Ngadi, Y., Jones, N., Paton-Walsh, C., Hadji-Lazaro, J., Vigouroux, C., De Mazière, M., Metzger, J.-M., Mahieu, E., Servais, C., Hase, F., Schneider, M., Clerbaux, C., and Coheur, P.-F.: Acetylene (C_2H_2) and hydrogen cyanide (HCN) from IASI satellite observations: global distributions, validation, and comparison with model, Atmos. Chem. Phys., 15, 10509-10527, doi:10.5194/acp-15-10509-2015, 2015.

Technical comments:
A revision of the English used could improve the transparency and clarity of the paper, particularly in the introduction.
It has been done.

Line 68, please include reference to Razavi et al., 2011 (first HCOOH retrievals from IASI).
The reference has been added.

Line 71, please include Gonzalez Abad et al., 2009 in ACE-FTS papers.
The reference has been added.

Line 98, please include citation about IASI CO2 retrievals.
This following reference has been added:
Crevoisier, C., Chédin, A., Matsueda, H., Machida, T., Armante, R., and Scott, N. A.: First year of upper tropospheric integrated content of CO_2 from IASI hyperspectral infrared observations, Atmos. Chem. Phys., 9, 4797-4810, doi:10.5194/acp-9-4797-2009, 2009.

Line 118, correct typo (Pommier et al., 2016).
Done

Line 141, actives to become active.
Changed.

Line 206, should read "Both biases are however" instead of "Both biases is howeve"
It reads now:
"The effects of both biases are, however, limited since most of HCOOH…"

Line 282, please specify which other studies.
This information is now available (in bold) in the following sentence:
"For the other regions, in addition to the values from Akagi et al. (2011), emission ratios were similarly calculated from emission factors given in other studies **(listed in Table 3)**."

Figure 2, include units in plots.

Figure 4, please include units in plots.
Figs 2 and 4 now include units, as hereafter:

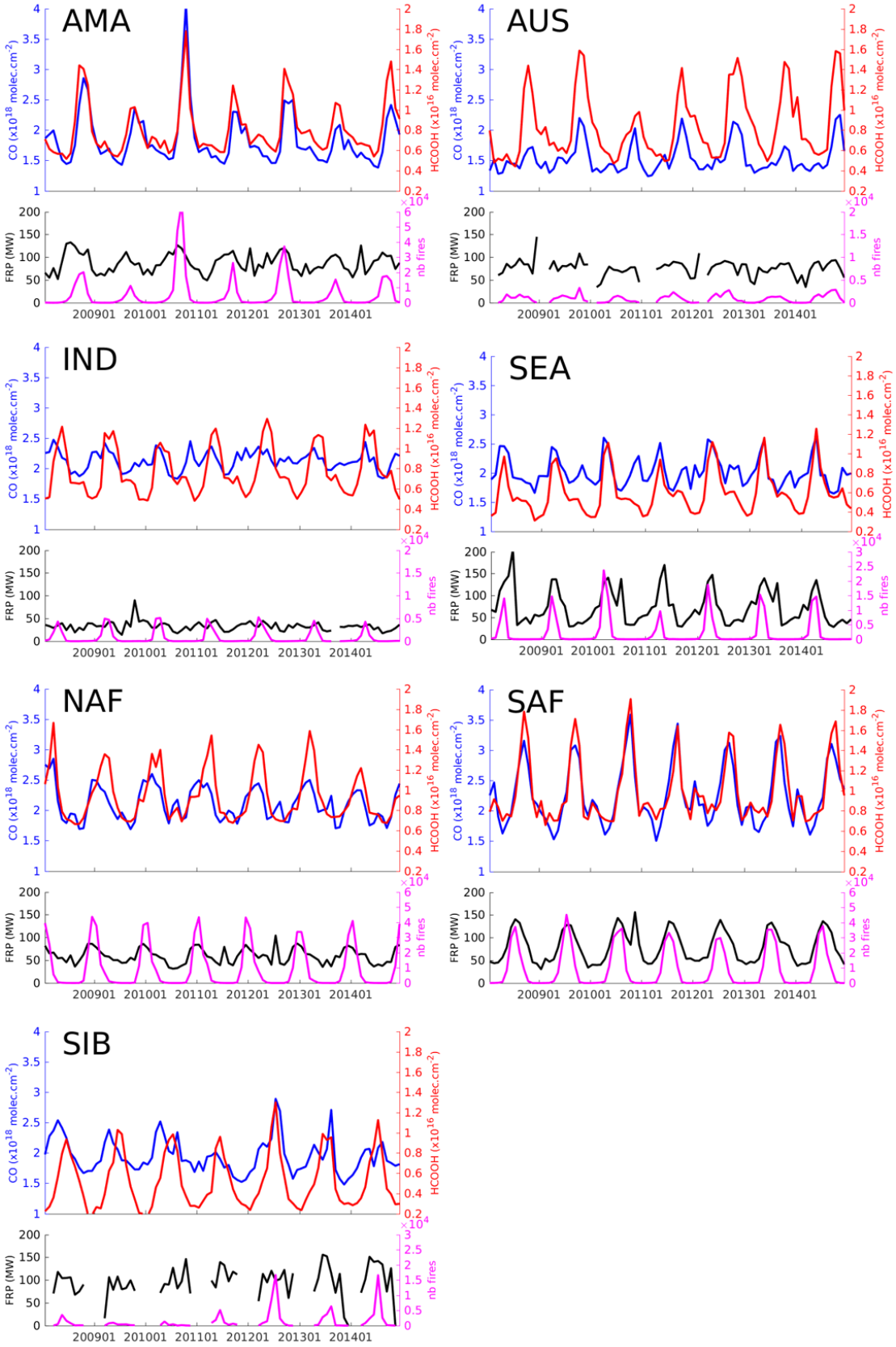

Figure 2: Time-series from 2008 to 2014 of the monthly means of IASI CO (blue) and HCOOH (red) total columns in 10^{18} molec/cm^2 and in 10^{16} molec/cm^2, respectively, FRP (black) in MegaWatts and the number of fires (magenta) from

MODIS over the seven regions (AMA=Amazonia, AUS=Australia, IND = India, SEA = Southern East Asia, NAF= Northern Africa, SAF= Southern Africa, SIB= Siberia).

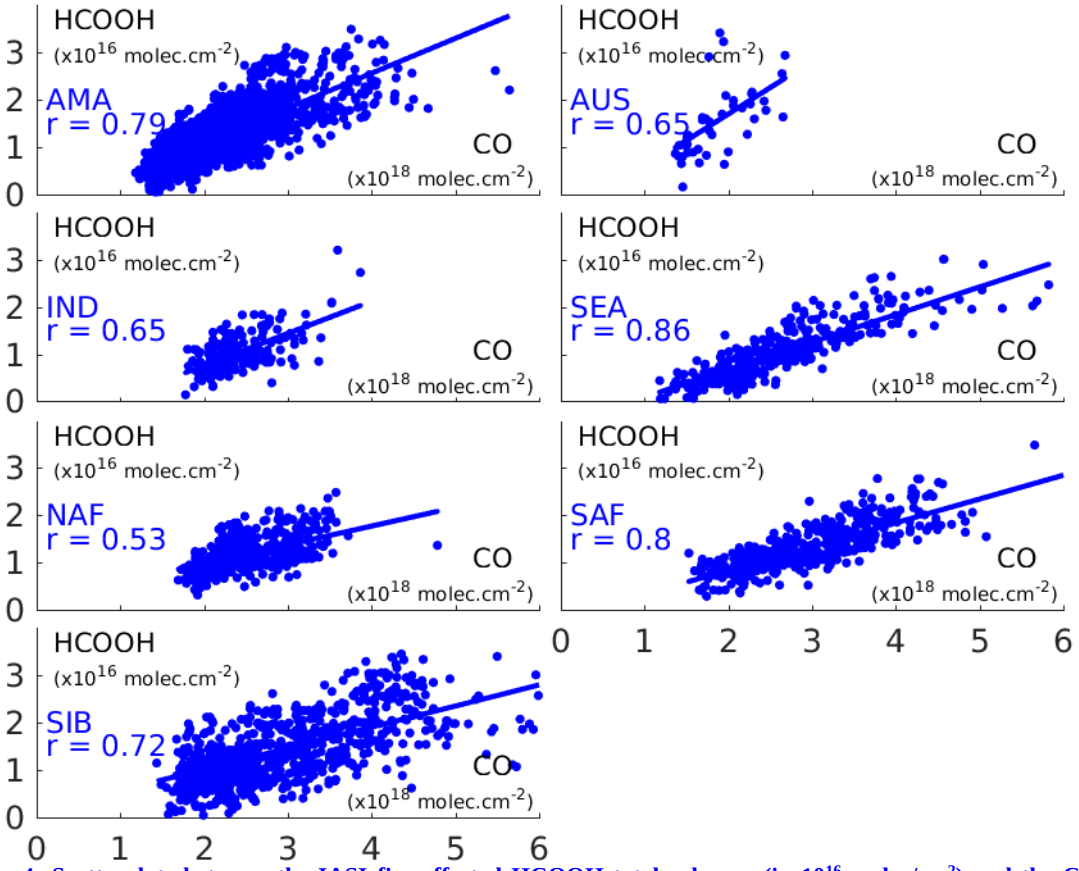

Figure 4: Scatterplots between the IASI fire-affected HCOOH total columns (in 10^{16} molec/cm^2) and the CO total columns (in 10^{18} molec/cm^2) over the seven regions (AMA=Amazonia, AUS=Australia, IND = India, SEA = Southern East Asia, NAF= Northern Africa, SAF= Southern Africa, SIB= Siberia).The linear regression is represented by the blue line and the correlation coefficient is also provided for each region.